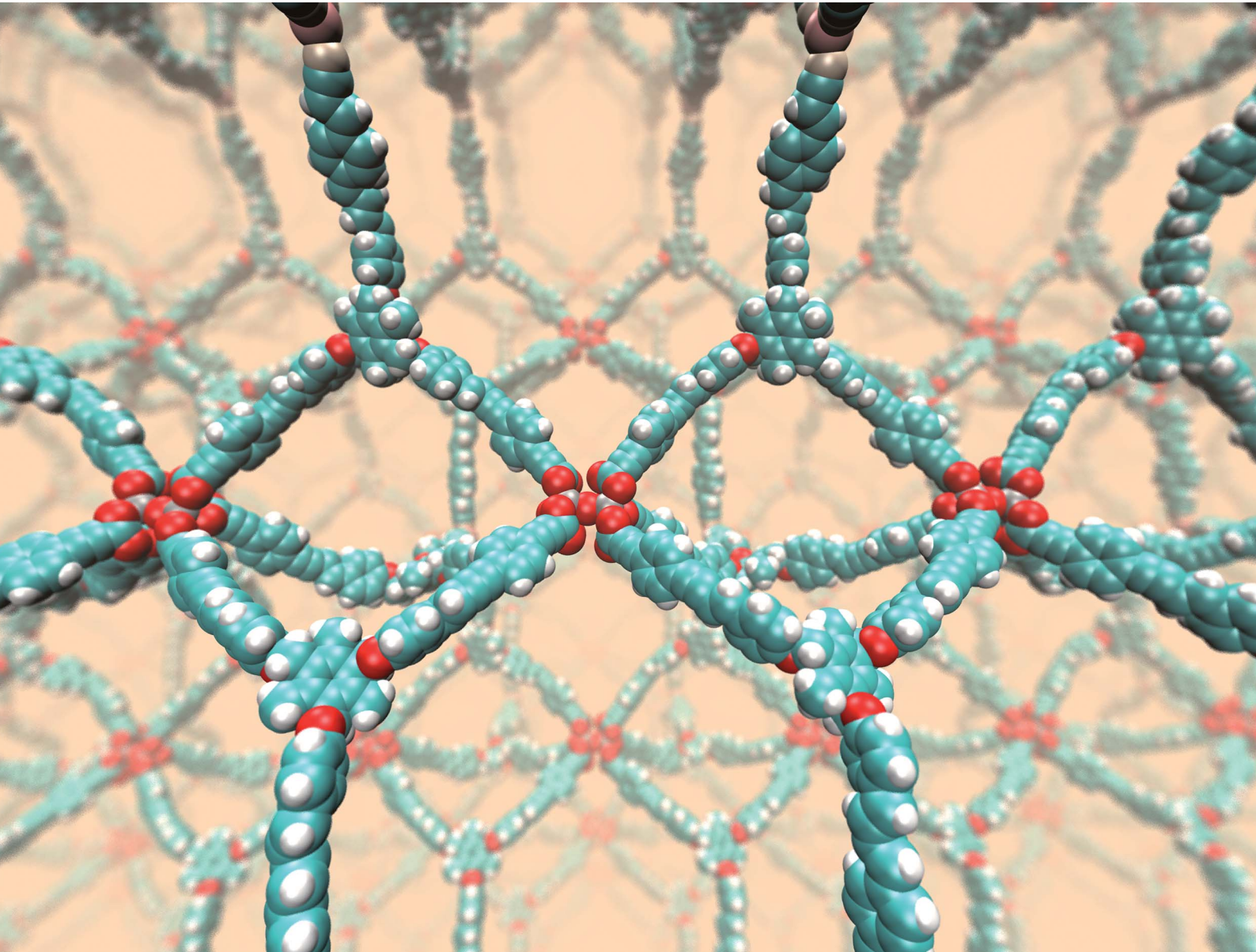
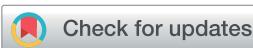


Digital Discovery

rsc.li/digitaldiscovery



ISSN 2635-098X



Cite this: *Digital Discovery*, 2024, **3**, 449

Received 15th January 2024
Accepted 7th February 2024

DOI: 10.1039/d4dd00020j
rsc.li/digitaldiscovery

Artificial intelligence holds promise to improve materials discovery. GFlowNets are an emerging deep learning algorithm with many applications in AI-assisted discovery. Using GFlowNets, we generate porous reticular materials, such as Metal Organic Frameworks and Covalent Organic Frameworks, for applications in carbon dioxide capture. We introduce a new Python package (matgfn) to train and sample GFlowNets. We use matgfn to generate the matgfn-rm dataset of novel and diverse reticular materials with gravimetric surface area above $5000 \text{ m}^2 \text{ g}^{-1}$. We calculate single- and two-component gas adsorption isotherms for the top-100 candidates in matgfn-rm. These candidates are novel compared to the state-of-art ARC-MOF dataset and rank in the 90th percentile in terms of working capacity compared to the CoRE2019 dataset. We identify 13 materials with CO_2 working capacity outperforming all materials in CoRE2019. After further analysis and structural relaxation, two outperforming materials remain.

1 Introduction

Artificial intelligence (AI) holds promise to improve the scientific method^{1,2} and to accelerate scientific discovery. Applied to materials,³ AI unlocks vast search spaces and enables novel applications in pharmaceuticals,^{3–6} batteries or carbon capture.⁷

Reticular materials⁸ such as Metal–Organic Frameworks (MOFs) and Covalent Organic Frameworks (COFs) are extended periodic structures connected *via* strong bonds.⁹ They are synthesized by connecting building blocks known as secondary building units to form three-dimensional periodic structures.¹⁰ By choosing the building blocks, the properties of a reticular material can be tuned to support many applications.⁸

Reticular materials with high gravimetric surface area are particularly useful for applications in carbon capture, since

carbon dioxide molecules adsorb at the internal surface area.¹¹ The larger the gravimetric surface area, the more gas molecules can be adsorbed per gram of material.

In this work, we use GFlowNets to generate reticular materials with high gravimetric surface area for applications in carbon capture. Our key contributions are:

(1) The matgfn Python library for training and sampling using GFlowNets.

(2) A workflow using matgfn to generate reticular materials using secondary building units.

(3) The matgfn-rm dataset of diverse and novel reticular materials with total internal surface area higher than $5000 \text{ m}^2 \text{ g}^{-1}$. The top-100 candidates are novel compared to the reference ARC-MOF dataset, rank in the 90th percentile in terms of simulated working capacity compared to the CoRE2019 dataset. We identify 13 materials with CO_2 working capacity outperforming all materials in CoRE2019. After further analysis and structural relaxation, 2 outperforming materials remain.

The code and dataset is available at <http://github.com/flaviucipcigan/matgfn> and archived on Zenodo.¹²

2 Background and related work

2.1 Generative flow networks

GFlowNets^{13,14} are an emerging machine learning algorithm with many applications in AI-assisted materials discovery.¹⁵ GFlowNets learn to generate composite objects \underline{x} by sampling from an unnormalised distribution $p(\underline{x}) \propto R(\underline{x})$ where $R(\underline{x})$ is a user-specified positive reward function. A composite object \underline{x} consists of symbols drawn from a vocabulary and relationships between those symbols. For example, \underline{x} can be a sequence $\underline{x} = [x_1, x_2, \dots, x_n]$ or a graph. The object \underline{x} is built by through Markov decision process restricted to a directed acyclic graph. Transition probabilities $p(x_i + 1 | \underline{x})$ are approximated by a neural network policy. GFlowNets need fewer evaluations of the reward function to generate samples with high reward, novelty and diversity when compared to alternatives such as Markov Chain

^aIBM Research Europe, UK. E-mail: flaviu.cipcigan@ibm.com

^bScience and Technologies Facilities Council, UK

^cIBM Research, Brazil

† Electronic supplementary information (ESI) available. See DOI: <https://doi.org/10.1039/d4dd00020j>



Monte Carlo, Proximal Policy Optimisation or Bayesian Optimisation.¹³

2.2 Building hypothetical reticular frameworks

Trillions of hypothetical frameworks such as MOFs or COFs can be generated by placing secondary building units¹⁰ into nodes and edges of a three dimensional topology.¹⁶ A secondary building unit is an organic molecule or a coordination compound (a metal linked to organic atoms). A topology is a three dimensional arrangement of nodes and edges. Replacing nodes and edges with secondary building units results in a three dimensional point cloud of atoms connected by covalent or metal–organic bonds. We use the pormake secondary building units¹⁷ and topology codes from the reticular chemistry structure resource.¹⁶ Previously, deep autoencoders¹⁸ and evolutionary methods¹⁷ have been used to generate frameworks using this approach.

2.3 Reference datasets

We use two reference datasets in this work. These datasets are not used for training models, but as comparison once training is done, as GFlowNet generates candidates using just a reward function. The CoRE2019 dataset¹⁹ consists of 12 023 metal–organic frameworks with carbon dioxide uptake properties calculated by Moosavi *et al.*²⁰ using Grand Canonical Monte Carlo. ARC-MOF (reported in 2022)²¹ is a collection of MOFs from previous MOF datasets, containing both experimental and hypothetical MOFs. We used the 521 380 structures that passed the structure checking protocol of Bruner *et al.* 2023,²¹ minus one structure which would give an error in our analysis.

3 Generating reticular frameworks with GFlowNets

3.1 Python package

We built a Python library called matgfn to train and sample GFlowNets. The library is built on top of PyTorch²² and Gymnasium²³ and prioritises ease of use and code readability. We intend for matgfn to be a general Python package for generation of diverse types of materials from small molecules to framework materials. Architecturally, matgfn separates sampling, loss calculation, optimisation, and environment definition as modular Python classes. Each can be modified individually, to implement off-policy training or use improved losses, for example. We note similar architectural choices for torchgfn.²⁴

3.2 Environment for reticular framework generation

We configure a GFlowNet environment to build string sequences made out of text tokens. Those text tokens start with either an N, representing a node building block, or an E, representing an edge building block. For example, one of the potential generated sequences is ["N577", "N238", "N194", "E5", "E3", "E74"]. We use building blocks in the pormake database. The string sequences

are transformed to a Crystallographic Information File (*.cif) by pormake to create a reticular framework. Not all strings create valid materials. Thus, during generation, building blocks were restricted such that (a) each topology had the correct number of nodes and edges, (b) the building blocks were placed in the correct order and (c) each slot had a compatible building block.

Block compatibility was assessed as follows. For each slot in each topology, we pre-calculate a list of allowed building blocks. We allow only building blocks whose (a) number of attachment points is equal to the number of attachment points for the slot and (b) the RMSD between the block and the geometry is less than 0.3 Å. The RMSD is calculated using pormake's locator class by finding the best fit between a building block and a slot. At every generation step, the GFlowNet policy is set to zero for any block that is not allowed.

3.3 Reward

We calculate the Gravimetric Surface Area GSA in $\text{m}^2 \text{ g}^{-1}$ with Zeo++²⁵ during the training loop of the GFlowNet. We configure Zeo++ with a probe radius of 1.525 Å and 2000 samples. The GFlowNet is given the following reward:

$$R(x) = \mathcal{H}(GSA(x) - C) \times \exp\left(\frac{GSA(x) - C}{C}\right) \quad (1)$$

where $\mathcal{H}(x)$ is the Heaviside step function $\mathcal{H}(x)(x) = 0$ if $x < 0$, 1 if $x \geq 0$ and C is a cutoff. Zeo++ and pormake sometimes raise errors due to large distances between atoms. The reward is zero when an error occurred to encourage the GFlowNet to avoid materials with unrealistic bond lengths.

3.4 Relationship with CO_2 capture

We demonstrate that the gravimetric surface area predicts CO_2 uptake by analysing approximately 30 000 MOFs from three databases: CoRE2019,¹⁹ ARABG²⁶ and BW20K.²⁷ We performed univariate linear regression of CO_2 uptake at 16 bar using each of the geometric and chemical descriptors. The best performing descriptor was the gravimetric surface area with coefficient of determination is 0.88, RMSE is 2.41 mol kg^{-1} and Spearman's rank correlation coefficient of 0.97. Fig. 1 shows the CO_2 uptake

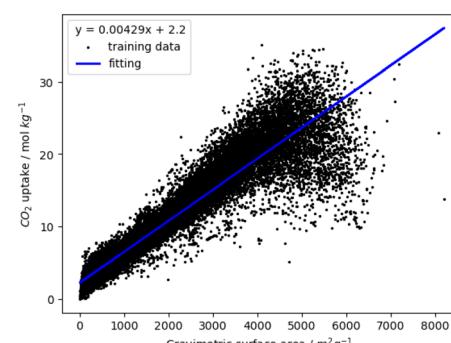


Fig. 1 Regression of simulated high pressure CO_2 uptake to gravimetric surface area.



as a function of gravimetric surface area. We validated the regression using 50 rounds of 10-fold cross validation, with each cross-validation consisting of an 80–20 split between training and test data. The mean coefficient of determination is 0.88 ± 0.0002 and mean RMSE is $2.41 \pm 0.022 \text{ mol kg}^{-1}$. The training and test values of coefficient of determination and RMSE are the same to two decimal places and the standard deviation of these metrics during cross validation are very small which shows that the correlation is robust and stable.

4 The matgfn-rm dataset

4.1 Training

We trained a GFlowNet using trajectory balance loss²⁸ and an LSTM policy. Each token was embedded using an embedding size of 32 and passed through an LSTM with two hidden layers of size 16. Finally, a MLP with one hidden layer of size 8 is used to compute the forward and backward policies as a single output vector. We use a learning rate of 5×10^{-3} for both the policy and the partition function. We train for a maximum of 100 000 episodes and stop when the mean loss over 10 000 episodes is lower than 1.8. We note that hyperparameter optimisation will likely improve the results.

The GFlowNet is trained from a reward rather than from x, y pairs (such as the case of supervised learning). Thus, data splitting methods are not relevant since there is no training set. An equivalent in sequential decision making is the exploration strategy, which in our case was on-policy.

Eleven topologies were chosen: CDZ-E, CLD-E, EFT, FFC, TSG, TFF, ASC, DMG, DNQ, FSO, URJ. These topologies were chosen because they were the fastest for which pormake can construct a MOF among the wider-known topologies. There is no limitation in using other topologies and thus further work can sample over a wider set of topologies or train a single, universal GFlowNet which chooses topology as one of its actions.

For each topology, two GFlowNets were trained, one with edges and one without. In pormake, each topology has two ways of constructing a MOF: with or without edges. To be comprehensive in our experiments, we trained a GFlowNet for each case. To avoid cherry-picking, we report all our results. For gravimetric surface area as a proxy, topologies with edges often outperform those without, as shown in ESI.†

Each trained GFlowNet (both with and without edges) was sampled between 70 000 and 120 000 times. The number of samples varies depending on the time taken to calculate the reward, and the sampler was given a fixed wall-time. These samples were de-duplicated and combined with those seen during training with a non-zero reward, thus forming the matgfn-rm dataset containing 1 709 126 items. The dataset is reported in the dataset/dataset.json file of matgfn.

4.2 Diversity and novelty analysis

To assess diversity and novelty, we compare the whole matgfn-rm to the ARC-MOF dataset. We first compute the average minimum distance (AMD) descriptor²⁹ of length 100 for each

CIF file in both datasets. This descriptor uniquely identifies crystal structures and is a continuous metric, meaning that the distance (measured using the Chebyshev metric) is zero for similar crystals. We embed the AMD to two dimensions using t-SNE, implemented in openTSNE,³⁰ using the Chebyshev distance metric and nearest neighbour descent.³¹ Fig. 2 shows the result. The matgfn-rm materials are separated from most materials from ARC-MOF. This indicates the generated materials are novel compared to existing datasets. To further assess novelty, we define the following distance metric given a dataset \mathbb{D} :

$$D(x; \mathbb{D}) = \min_{d \in \mathbb{D}} \| \text{AMD}(x) - \text{AMD}(d) \|_{\infty} \quad (2)$$

Intuitively, this metric is the distance to the closest point in the reference dataset. Using scikit-learn³²'s NearestNeighbor, we compute this metric for all materials in matgfn-rm with respect to ARC-MOF. Fig. 4 shows a histogram of $D(x)$ and a violin plot of the gravimetric surface area in each bin. As the distance metric increases, the mean gravimetric surface area also increases, indicating that the “further” away a generated structure is from the reference dataset, the higher the gravimetric surface area. In ESI, Fig. S15† we present a similar analysis that only considers the top-100 structures in ARC-MOF and matgfn-rm. Given that the distribution of gravimetric surface area in the top-100 in those two datasets shows no overlap, the T-SNE embedding shows almost perfect separation, again indicating novelty of the generated top-100.

4.3 Simulated CO₂ capture performance

In order to confirm the expectation of efficient CO₂ capture from an adsorption proxy (*i.e.*, the gravimetric surface area), we run physics-based Grand Canonical Monte Carlo simulations

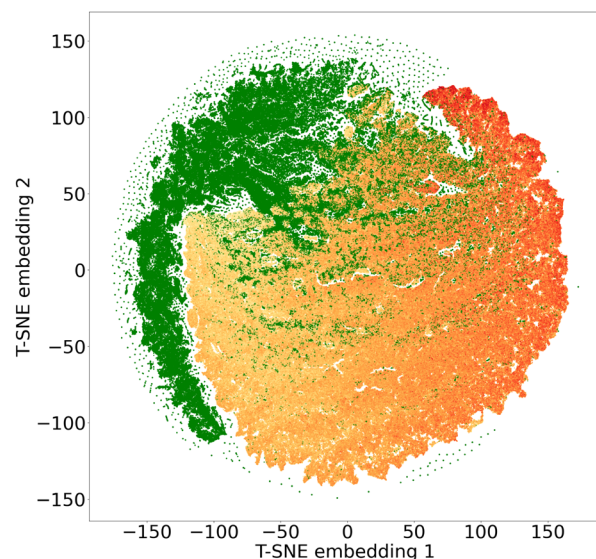


Fig. 2 Two dimensional t-SNE embedding of the average minimum distance of ARC-MOF (green), and matgfn-rm (yellow to orange) materials. The colours in the matgfn-rm dataset are proportional to the reward, with light yellow signifying low reward and dark orange high reward.



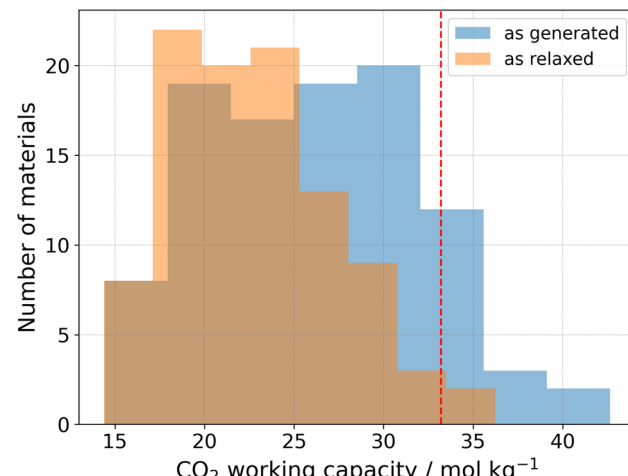


Fig. 3 Distribution of simulated CO_2 working capacity for the top-100 matgfn-rm materials as generated (blue) and after relaxation (orange). The red dashed line represents the highest working capacity found in the CoRE2019 dataset, which is surpassed by 13 (2) of the top-100 matgfn-rm materials before (after) structural relaxation.

for the top-100 generated materials in the matgfn-rm dataset.^{33,34} We simulated single-component adsorption isotherms for pure CO_2 , from which we extract the working capacity. All simulations were performed at 300 K, with pressures ranging from 0.15 to 16 bar. The working capacity was calculated as the difference in uptake of CO_2 between the highest and lowest pressures. Fig. 3 shows (in blue) the distribution of working capacity for the top-100 matgfn-rm materials. All top-100 materials exhibit very high CO_2 working capacities, corresponding to the 90th percentile of the experimentally-realised CoRE2019 dataset.²⁰ They are (modestly) more selective towards CO_2 than N_2 , achieving selectivity between 1 and 4 (not shown). Thirteen of the top-100 matgfn-rm materials have working capacities that are higher than all materials found in

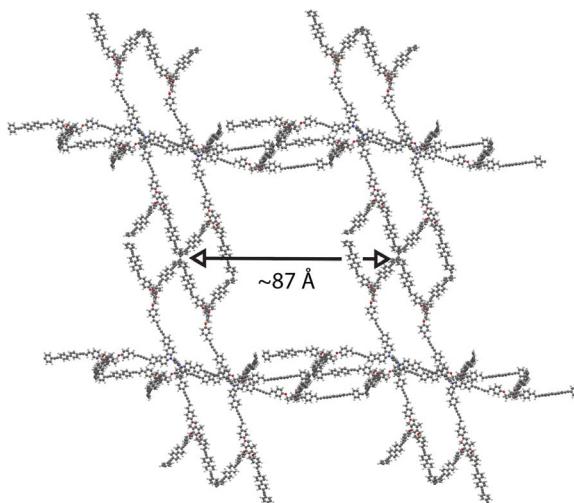


Fig. 5 A render of the relaxed structure of 005-ffc-10217, the highest performing structure in the matgfn-rm dataset. We show here the $2 \times 2 \times 2$ supercell.

the CoRE2019 dataset. In particular, we highlight in Fig. 5 the covalent organic framework 005-ffc-10217 that achieved the highest CO_2 working capacity of approximately 43 mol kg^{-1} .

4.4 Relaxation and validity checks

Due to the hypothetical nature of the generated MOFs, the crystalline structures are not guaranteed to be perfect. We therefore used the mofchecker library³⁵ to perform basic consistency checks on the generated CIFs. According to mofchecker, all of the top-100 matgfn-rm are porous (metal-) organic materials. However, due to the hypothetical interatomic distances sometimes being larger (or shorter) than the typical bond lengths, some atoms are flagged as either over- or under-coordinated. In order to obtain a more realistic structure, we

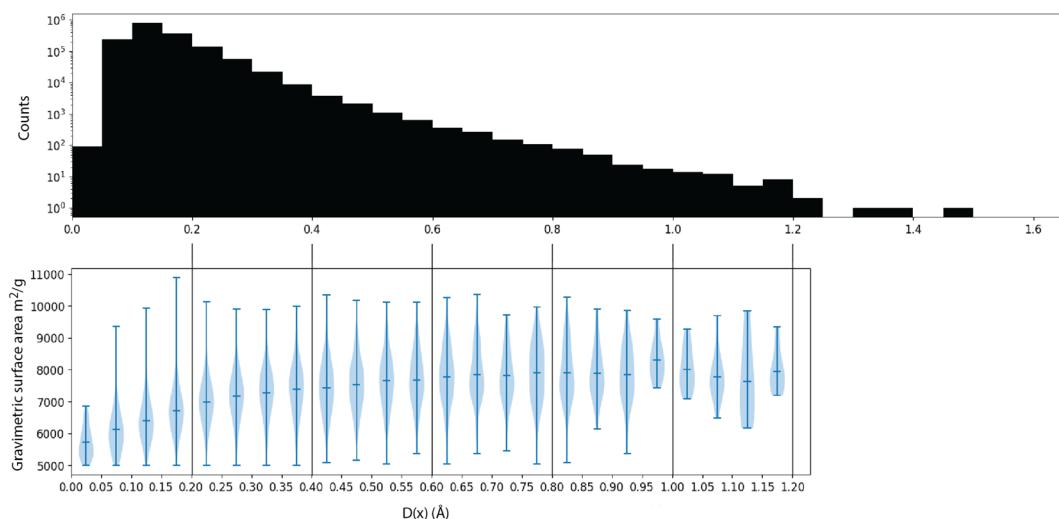


Fig. 4 (Top) A histogram of the distance metric $D(x)$ in eqn (2) with respect to the ARC-MOF dataset. (Bottom) For each bin in the histogram, a violin plot of the gravimetric surface area of elements in that bin, showing that materials with higher distance to the reference dataset have higher gravimetric surface areas.

performed atomic coordinate and unit cell relaxation using the CHGNet³⁶ interatomic potential. Relaxing the structures solves most of the structural problems, with 98% presenting neither atomic overlaps nor over-coordination of C, N and H atoms, respectively. In particular, for the high-performing 005-ffc-10217 structure, relaxation led to a 23% reduction in the unit cell volume, bringing the CO₂ working capacity down to 36.2 mol kg⁻¹, which is still larger than those found in the CoRE2019 dataset. In Fig. 3, we show (in orange) the distribution of working capacity for the top-100 matgfn-rm materials after structural relaxation. Despite the overall reduction of the working capacity due to unit cell shrinkage, the subset remains in the 90th percentile of the CoRE2019 dataset. Two of the relaxed top-100 matgfn-rm materials have higher working capacities than any material found in the CoRE2019 dataset. The relaxed pore size of 005-ffc-10217 is approximately 87 Å. Structural relaxation changes the average minimum distance descriptors by a small amount and thus the diversity analysis still holds. See ESI, Fig. S14† for an illustration of the effect of relaxation on the t-SNE embeddings.

5 Discussion

The ultimate goal of computer-aided discovery is materials with improved real-world performance. In carbon capture applications the choice of materials should consider figures-of-merit at the process level.^{37,38} Molecular-level metrics, such as the gravimetric surface area, working capacity, heat of adsorption and molecular selectivity, are useful, accessible proxies that help bridge the scale gap and provide an early prioritisation of candidates. Out of all the options, we chose the widely used working capacity as a representative metric, which was maximised despite not having been intentionally optimised for. Molecular selectivity is another key figure-of-merit in carbon dioxide capture. The realization that we have generated reticular structures with selectivity greater than one, even though selectivity was not explicitly included in the reward function, indicates the potential of GFlowNets for creating novel materials for application in chemical separations. To further improve the candidates, selectivity, working capacity or even process-level metrics can be included in the reward function, possibly using an active-learning approach.³⁹

Algorithmic approaches can also push the performance further. Key ones would be hyperparameter optimisation, improved exploration (e.g. using Thompson Sampling⁴⁰), training a single GFlowNet for all topologies, improved losses⁴¹ and multi-objective reward functions^{42–44} that enable a more holistic evaluation of the material performance and usability, including stability and synthesisability dimensions.⁴⁵ All these are possible using the framework presented here and thus our paper opens up all these possibilities for follow-up to obtain use-able, real-world materials.

6 Conclusion

In summary, we built a workflow using GFlowNets to generate diverse and novel reticular frameworks with gravimetric surface

area greater than 5000 m² g⁻¹. As a key result, the top-100 candidates of the resulting matgfn-rm dataset have working capacities in the top 90th percentile of CoRE2019 reference dataset. Moreover, 2 of the top-100 matgfn-rm materials have working capacities that are higher than all materials found in the CoRE2019 dataset. After further analysis and structural relaxation, 2 outperforming materials remain. Further work is needed to confirm the stability and synthesizability of the materials generated in our study. Nevertheless, our results clearly demonstrate the potential of GFlowNets for materials discovery in carbon capture applications.

Data availability

Matgfn is available at <https://github.com/flaviucipcigan/matgfn> and archived on Zenodo at <https://zenodo.org/records/10246465>. In the repository, the notebook to generate reticular materials is at notebooks/reticular_materials.ipynb, the training script at dataset/train_agent.py, the dataset in dataset/dataset.json and the analysis scripts in multiple python files in dataset/.

Author contributions

Flaviu Cipcigan: project: conceptualisation, project administration. Paper: writing – coordination, writing – original draft, writing – review & editing. Software: main author of matgfn, contributor to MOF application code, results: methodology, experiments, formal analysis, validation, diversity analysis of matgfn-rm. Jonathan Booth: project: project administration, trained GFlowNets on MOF topologies paper: writing – MOF result section, writing – review & editing. Software: created reward function and other necessary code for MOF application of GFlowNets results: methodology, experiments, formal analysis, validation. Rodrigo Neumann Barros Ferreira: paper: writing – original draft, writing – review & editing. Results: validation and simulations of matgfn-rm dataset. Carine Ribeiro dos Santos: results: validation and simulations of matgfn-rm dataset. Mathias Steiner: project: project administration. Paper: writing – original draft, writing – review & editing.

Conflicts of interest

There are no conflicts of interest to declare.

Acknowledgements

We thank Dan Cunningham and Won Kyung Lee for valuable comments on the manuscript. Flaviu Cipcigan and Jonathan Booth were supported by the Hartree National Centre for Digital Innovation, a collaboration between STFC and IBM.

Notes and references

† Here, we conceptualise materials broadly to include molecules, proteins, crystals and complex materials.



- 1 T. Hey, S. Tansley and K. Tolle, *The Fourth Paradigm: Data-Intensive Scientific Discovery*, Microsoft Research, 2009.
- 2 A. Agrawal and A. N. Choudhary, *APL Mater.*, 2016, **4**, 053208.
- 3 P. Das, T. Sercu, K. Wadhawan, I. Padhi, S. Gehrmann, F. Cipcigan, V. Chenthamarakshan, H. Strobelt, C. dos Santos, P.-Y. Chen, Y. Y. Yang, J. P. K. Tan, J. Hedrick, J. Crain and A. Mojsilovic, *Nat. Biomed. Eng.*, 2021, **5**, 613–623.
- 4 D. Crusius, J. R. Schnell, F. Cipcigan and P. C. Biggin, *Digital Discovery*, 2023, **2**, 1163–1177.
- 5 K. Hammond, F. Cipcigan, K. A. Nahas, V. Losasso, H. Lewis, J. Cama, F. Martelli, P. W. Simcock, M. Fletcher, J. Ravi, P. J. Stansfeld, S. Pagliara, B. W. Hoogenboom, U. F. Keyser, M. S. P. Sansom, J. Crain and M. G. Ryadnov, *ACS Nano*, 2021, **15**, 9679–9689.
- 6 F. Cipcigan, P. Smith, J. Crain, A. Hogner, L. D. Maria, A. Llinas and E. Ratkova, *J. Chem. Inf. Model.*, 2020, **61**, 263–269.
- 7 J. L. McDonagh, B. H. Wunsch, S. Zavitsanou, A. Harrison, B. Elmegreen, S. Gifford, T. van Kessel and F. Cipcigan, *arXiv*, 2023, preprint, arXiv:2303.14223, DOI: [10.48550/arXiv.2303.14223](https://doi.org/10.48550/arXiv.2303.14223).
- 8 O. M. Yaghi, M. J. Kalmutzki and C. S. Diercks, *Introduction to reticular chemistry: metal-organic frameworks and covalent organic frameworks*, John Wiley & Sons, 2019.
- 9 R. Freund, S. Canossa, S. M. Cohen, W. Yan, H. Deng, V. Guillerm, M. Eddaoudi, D. G. Madden, D. Fairnjimenez, H. Lyu, L. K. Macreadie, Z. Ji, Y. Zhang, B. Wang, F. Haase, C. Wöll, O. Zaremba, J. Andreo, S. Wuttke and C. S. Diercks, *Angew. Chem.*, 2021, **60**(45), 23946–23974.
- 10 M. J. Kalmutzki, N. Hanikel and O. M. Yaghi, *Sci. Adv.*, 2018, **4**, eaat9180.
- 11 O. K. Farha, I. Eryazici, N. C. Jeong, B. G. Hauser, C. E. Wilmer, A. A. Sarjeant, R. Q. Snurr, S. T. Nguyen, A. Özgür Yazaydin and J. T. Hupp, *J. Am. Chem. Soc.*, 2012, **134**, 15016–15021.
- 12 F. Cipcigan, *Zenodo archive for flaviucipcigan/matgfn*, 2023, DOI: [10.5281/zenodo.10246465](https://doi.org/10.5281/zenodo.10246465).
- 13 E. Bengio, M. Jain, M. Korablyov, D. Precup and Y. Bengio, *arXiv*, 2021, preprint, arXiv:2106.04399v2, DOI: [10.48550/arXiv.2106.04399](https://doi.org/10.48550/arXiv.2106.04399).
- 14 Y. Bengio, T. Deleu, E. J. Hu, S. Lahlou, M. Tiwari and E. Bengio, *arXiv*, 2021, preprint, arXiv:2111.09266, DOI: [10.48550/arXiv.2111.09266](https://doi.org/10.48550/arXiv.2111.09266).
- 15 M. Jain, T. Deleu, J. S. Hartford, C.-H. Liu, A. Hernández-García and Y. Bengio, *arXiv*, 2023, preprint, arXiv:2302.00615, DOI: [10.48550/arXiv.2302.00615](https://doi.org/10.48550/arXiv.2302.00615).
- 16 M. O'Keeffe, M. A. Peskov, S. J. Ramsden and O. M. Yaghi, *Acc. Chem. Res.*, 2008, **41**, 1782–1789.
- 17 S. Lee, B. Kim, H. Cho, H. Lee, S. Y. Lee, E. S. Cho and J. Kim, *ACS Appl. Mater. Interfaces*, 2021, **13**, 23647–23654.
- 18 Z. Yao, B. Sánchez-Lengeling, N. S. Bobbitt, B. J. Bucior, S. G. H. Kumar, S. P. Collins, T. Burns, T. K. Woo, O. K. Farha, R. Q. Snurr and A. Aspuru-Guzik, *Nat. Mach. Intell.*, 2021, **3**, 76–86.
- 19 Y. G. Chung, E. Haldoupis, B. J. Bucior, M. Haranczyk, S. Lee, H. Zhang, K. D. Vogiatzis, M. Milisavljevic, S. Ling, J. S. Camp, B. Slater, J. I. Siepmann, D. S. Sholl and R. Q. Snurr, *J. Chem. Eng. Data*, 2019, **64**, 5985–5998.
- 20 S. M. Moosavi, A. Nandy, K. M. Jablonka, D. Ongari, J. P. Janet, P. G. Boyd, Y. Lee, B. Smit and H. J. Kulik, *Nat. Commun.*, 2020, **11**, 4068.
- 21 J. Burner, J. Luo, A. White, A. Mirmiran, O. Kwon, P. G. Boyd, S. Maley, M. Gibaldi, S. Simrod, V. Ogden and T. K. Woo, *Chem. Mater.*, 2023, **35**, 900–916.
- 22 A. Paszke, S. Gross, F. Massa, A. Lerer, J. Bradbury, G. Chanan, T. Killeen, Z. Lin, N. Gimelshein, L. Antiga, A. Desmaison, A. Kopf, E. Z. Yang, Z. DeVito, M. Raison, A. Tejani, S. Chilamkurthy, B. Steiner, L. Fang, J. Bai and S. Chintala, *arXiv*, 2019, preprint, arXiv:1912.01703, DOI: [10.48550/arXiv.1912.01703](https://doi.org/10.48550/arXiv.1912.01703).
- 23 M. Towers, J. K. Terry, A. Kwiatkowski, J. U. Balis, G. d. Cola, T. Deleu, M. Goulão, A. Kallinteris, K. G. Arjun, M. Krimmel, R. Perez-Vicente, A. Pierré, S. Schulhoff, J. J. Tai, A. T. J. Shen and O. G. Younis, *Gymnasium*, 2023, <https://zenodo.org/record/8127025>.
- 24 S. Lahlou, J. D. Viviano, V. Schmidt and Y. Bengio, *torchgfn, A PyTorch GFlowNet library*, 2023.
- 25 T. F. Willems, C. H. Rycroft, M. Kazi, J. C. Meza and M. Haranczyk, *Microporous Mesoporous Mater.*, 2012, **149**, 134–141.
- 26 R. Anderson, E. Argueta, A. Biong and D. Gomez-Gualdrón, *Chem. Mater.*, 2018, **30**(18), 6325–6337.
- 27 P. G. Boyd, A. Chidambaram, E. García-Díez, C. P. Ireland, T. D. Daff, R. Bounds, A. Gladysiak, P. Schouwink, S. M. Moosavi, M. M. Maroto-Valer, J. A. Reimer, J. A. R. Navarro, T. K. Woo, S. Garcia, K. C. Stylianou and B. Smit, *Nature*, 2019, **576**, 253–256.
- 28 N. Malkin, M. Jain, E. Bengio, C. Sun and Y. Bengio, *Adv. Neural Inf. Process.*, 2022, **35**, 5955–5967.
- 29 D. Widdowson, M. M. Mosca, A. Pulido, A. I. Cooper and V. Kurlin, *MATCH Commun. Math. Comput. Chem.*, 2021, **87**, 529–559.
- 30 P. G. Poličar, M. Stražar and B. Zupan, *bioRxiv*, 2019, preprint, DOI: [10.1101/731877](https://doi.org/10.1101/731877).
- 31 W. Dong, C. Moses and K. Li, *Proceedings of the 20th International Conference on World Wide Web*, New York, NY, USA, 2011, pp. 577–586.
- 32 F. Pedregosa, G. Varoquaux, A. Gramfort, V. Michel, B. Thirion, O. Grisel, M. Blondel, P. Prettenhofer, R. Weiss, V. Dubourg, J. Vanderplas, A. Passos, D. Cournapeau, M. Brucher, M. Perrot and E. Duchesnay, *J. Mach. Learn. Res.*, 2011, **12**, 2825–2830.
- 33 R. Neumann Barros Ferreira, B. O Conchuir, T. Elengikal, B. Luan, R. L. Ohta, F. Lopes Oliveira, A. Mhadeshwar, J. Kalyanaraman, A. Sundaram, J. Falkowski *et al.*, *Proceedings of the 16th Greenhouse Gas Control Technologies Conference*, 2022.
- 34 F. L. Oliveira, C. Cleeton, R. Neumann Barros Ferreira, B. Luan, A. H. Farmahini, L. Sarkisov and M. Steiner, *Sci. Data*, 2023, **10**, 230.
- 35 K. M. Jablonka, 2023, <https://github.com/kjappelbaum/mofchecker>.



36 B. Deng, P. Zhong, K. Jun, J. Riebesell, K. Han, C. J. Bartel and G. Ceder, *Nat. Mach. Intell.*, 2023, 1–11.

37 D. Yancy-Caballero, K. T. Leperi, B. J. Bucior, R. K. Richardson, T. Islamoglu, O. K. Farha, F. You and R. Q. Snurr, *Mol. Syst. Des. Eng.*, 2020, 5, 1205–1218.

38 A. H. Farmahini, S. Krishnamurthy, D. Friedrich, S. Brandani and L. Sarkisov, *Chem. Rev.*, 2021, 121, 10666–10741.

39 M. Jain, E. Bengio, A.-H. Garcia, J. Rector-Brooks, B. F. P. Dossou, C. Ekbote, J. Fu, T. Zhang, M. Kilgour, D. Zhang, L. Simine, P. Das and Y. Bengio, *Biological Sequence Design with GFlowNets*, 2022, <https://arxiv.org/abs/2203.04115>.

40 J. Rector-Brooks, K. Madan, M. Jain, M. Korablyov, C.-H. Liu, S. Chandar, N. Malkin and Y. Bengio, *arXiv*, 2023, preprint, arXiv:2306.17693, DOI: [10.48550/arXiv.2306.17693](https://doi.org/10.48550/arXiv.2306.17693).

41 K. Madan, J. Rector-Brooks, M. Korablyov, E. Bengio, M. Jain, A. C. Nica, T. Bosc, Y. Bengio and N. Malkin, *International Conference on Machine Learning*, 2022.

42 M. Jain, S. C. Raparthy, A. Hernández-García, J. Rector-Brooks, Y. Bengio, S. Miret and E. Bengio, *International Conference on Machine Learning*, 2023, pp. 14631–14653.

43 B. Liu, Y. Feng, P. Stone and Q. Liu, *arXiv*, 2023, preprint, arXiv:2306.03792, DOI: [10.48550/arXiv.2306.03792](https://doi.org/10.48550/arXiv.2306.03792).

44 Y. He, X. Feng, C. Cheng, G. Ji, Y. Guo and J. Caverlee, *Proceedings of the ACM Web Conference*, 2022, 2022, pp. 2205–2215.

45 S. A. Mohamed, D. Zhao and J. Jiang, *Commun. Mater.*, 2023, 4, 79.

